Power Balance Analysis of Wendelstein 7-X Plasmas Using Profile Diagnostics

S.A. Bozhenkov[1], G. Fuchert[1], H. Niemann[1], M. Beurskens[1], Y. Feng[1], O.P. Ford[1], J. Geiger[1], M. Hirsch[1], U. Höfel[1], M.W. Jakubowski[1], J. Knauer[1], P. Kornejew[1], A. Langenberg[1], H.P. Laqua[1], H. Maassberg[1], N.B. Marushchenko[1], D. Moseev[1], N. Pablant[2], E. Pasch[1], K. Rahbarnia[1], T. Stange[1], J. Svensson[1], H. Trimino Mora[1], P. Valson[1], G. Wurden[3], D. Zhang[1], R.C. Wolf[1] and W7-X team

[1] *Max-Planck-Intitut für Plasmaphysik, Greifswald, Germany*

[2] *Princeton Plasma Physics Laboratory, Princeton, NJ, USA*

[3] *Los Alamos National Laboratory, Los Alamos, USA*

Introduction. In the first experimental campaign Wendelstein 7-X was equipped with 5 poloidal limiters and was operated in dedicated magnetic configurations with good flux surfaces in the scrape-off layer [1]. Plasma break-down and heating were provided by Electron Cyclotron Resonance Heating (ECRH) with up to 4.3 MW [2]. Electron temperatures of about 7 keV, ion temperatures of about 2 keV and electron densities of about $4 \cdot 10^{19}$ m^{-3} were achieved simultaneously [3]. In this contribution consistency of profile diagnostics with each other and with diamagnetic energy measurements is discussed. Afterwards a global power balance analysis and an estimation of the global energy confinement time are given.

Profile diagnostics. The main plasma parameters are measured with the following diagnostics: (i) Thomson scattering for a half profile of T_e and n_e at 10 spatial positions [5]; (ii) the absolutely calibrated Electron Cyclotron Emission (ECE) measures a full temperature profile with 32 channels [6]; (iii) an X-ray imaging crystal spectrometer (XICS) measures line integrated values of T_e and T_i from the emission of helium like Ar [8]; and (iv) a CO_2 dispersion interferometer measures the line integrated density close to the path of the Thomson scattering laser [7]. The diamagnetic plasma energy is measured with a diamagnetic loop which is corrected for induced currents and the reaction of the main coils system [9].

A comparison of T_e profiles from the three diagnostics averaged over a flat-top phase of one of the discharges is given in figure 2a. The ECE profiles are mapped by using the cold resonances and include calibration uncertainties. The XICS T_e profile was obtained by an inversion, the error bars represent the associated inversion uncertainty. The Thomson scattering profile is plotted without error bars, because the statistical errors are negligible and the systematic errors are presently being investigated. In this case the difference between the three T_e diagnostics is about 10%. In discharges with higher plasma pressure, a systematic difference between both halves of the ECE diagnostic and also between ECE and Thomson scattering is observed. A suitable mapping of ECE frequencies with plasma effects is under investigation. In figure 2a also an ion temperature profile from XICS is given. The T_i profile is very flat in the whole range

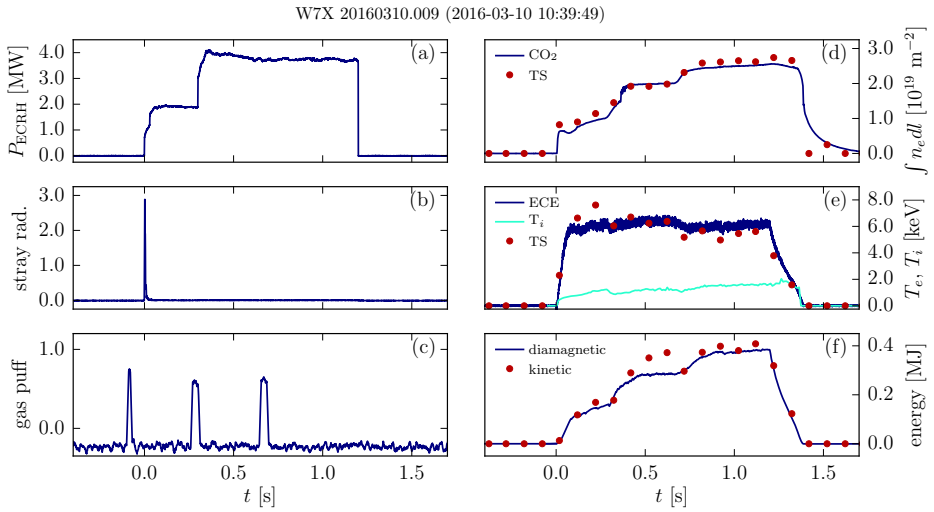

Figure 1: Overview of a W7-X discharge. (a) - ECRH power; (b) - microwave stray radiation by a sniffer probe; (c) - voltage of gas puff valves; (d) - line integrated density from the dispersion interferometer and Thomson scattering diagnostic; (e) - central T_e from ECE and Thomson scattering, central T_i from XICS; (f) - diamagnetic plasma energy and kinetic plasma energy from profile diagnostics.

of measurements and the uncertainty is negligible for the shown example .

Electron density profiles obtained from Thomson scattering in a discharge with increasing density are presented in figure 2b with statistical errors. Thomson scattering is absolutely calibrated with Raman scattering in nitrogen [5]. Such profiles can be used to compute the line integrated density and thus can be compared to the interferometer, figure 1d. Statistical analysis shows that the difference between the Thomson scattering and the interferometer is of the order of 10% and changes from day to day, which is likely due to changes in the laser alignment.

The kinetic plasma energy can be calculated from the profile measurements according to:

$$W_{\text{kin}} = \frac{3}{2}\int (n_e T_e + n_i T_i)\frac{dV}{dr}dr \tag{1}$$

The ion density profile n_i is presently assumed to be equal to n_e, because measurements of the average ion charge are not available yet. The volume derivative dV/dr and mapping to effective radii are taken for the vacuum configuration. VMEC equilibrium reconstructions for typical pressure profiles ($<\beta>\leq 0.4\%$) predict that the vacuum approximation overestimates the integral by less than 8%.

A comparison of kinetic energy calculated from the profile diagnostics with the diamagnetic energy measurements is presented in figure 1f. Statistical analysis of available data shows that the kinetic energy exceeds the diamagnetic one by about 25% on average. One possible reason for this difference is the assumption for the ion density. For example, 10% of carbon reduces the kinetic energy by 10%, and for 20% of carbon the reduction is about 17%.

Global power balance. The global power balance is the balance between heating power P_{ECRH}, radiated power P_{rad}, power deposited on the limiters P_{lim} and the change of the plasma energy:

$$P_{\text{ECRH}} - P_{\text{rad}} - P_{\text{lim}} - \frac{dW}{dt} = 0 \tag{2}$$

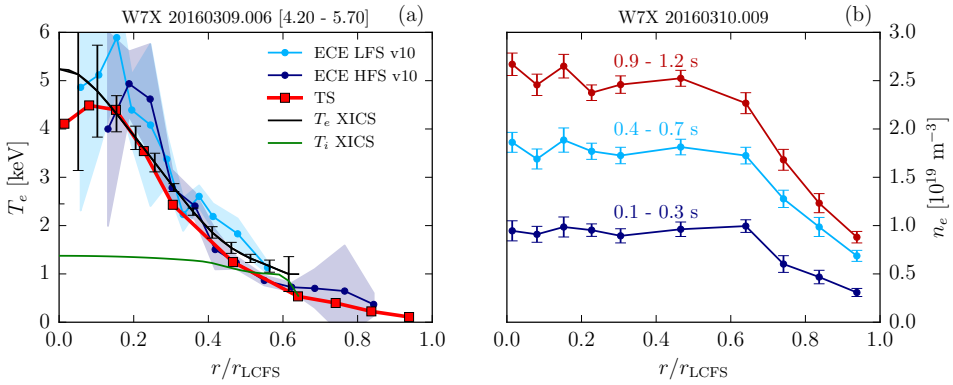

Figure 2: Typical temperature and density profiles. (a) - electron and ion temperature measured by ECE, Thomson scattering and XICS; (b) - electron density measured by Thomson scattering.

A preliminary estimation with the EMC3-EIRENE code indicates that under some conditions charge exchange neutrals can also make a noticeable contribution. This effect is still under investigation.

The ECRH heating power is measured inside the multibeam transmission line with an accuracy of about 10% by RF diodes and bolometers [2]. Typically after a plasma break down about 95–97% of the ECRH X2 power delivered to the vessel is absorbed by the plasma as verified by sniffer probes measuring the microwave stray radiation, figure 1b. The radiated power is measured with a bolometer system consisting of a horizontal and a vertical camera with 20 to 25 lines of sight [4]. The total radiated power is estimated assuming toroidal symmetry. Limiter heat fluxes are measured with two infrared cameras: one camera with a direct view on the limiter tiles from 3 to 5 (λ =3–5 μm) [13] in module 3 and the second one covering one half of all 9 limiter tiles in module 5 (λ =8–14 μm) [10]. The heat fluxes are reconstructed using the THEODOR code [12]. The total power intercepted by all five limiters can be obtained with a symmetry assumption.

An example of the power balance is given in figure 3. In figure 3a heating power, radiated power and power to the limiters are plotted. In this case the heating power was successively reduced, which also leads to an increase in the fraction of radiated power. The global power balance is shown in figure 3c. In this discharge, the power is accounted with an error of better than 20%, the mismatch decreases for lower heating powers. In general, it is found that for heating powers below about 1 MW the power balance is verified with an accuracy of about 10%, whereas for discharges with higher heating power the unaccounted power can reach almost 40%. This could be explained by an asymmetry of limiter heat fluxes in different modules. For high heating powers near-infrared cameras (λ =0.85–1 μm) in module 1 and 5 show much higher limiter temperature in module 1. The reason for the asymmetry is being investigated. The radiated power fraction in stable conditions, i.e. not in radiative collapse, is found to decrease with the heating power, figure 3d. For heating powers above about 1 MW the radiated power fraction is about 30%, whereas for lower powers higher fractions are also observed.

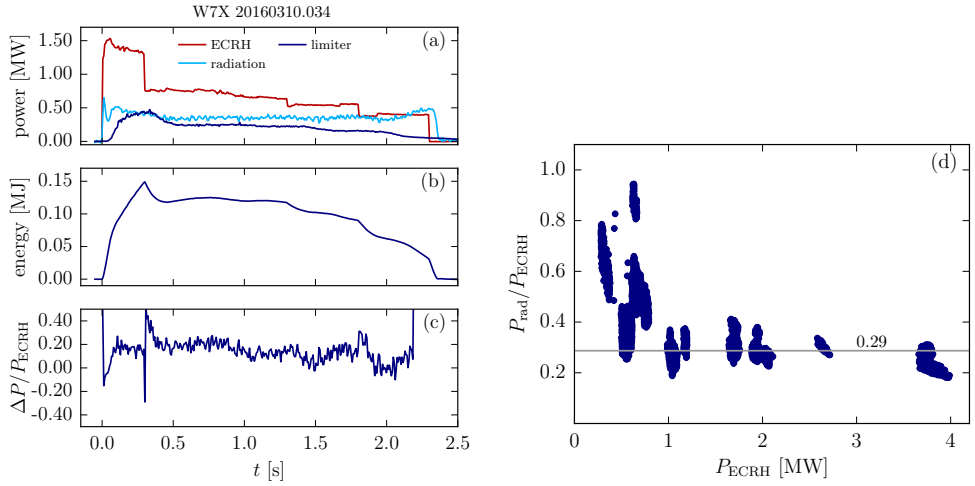

Figure 3: Power balance. (a) - heating and loss powers; (b) - plasma energy; (c) - power balance according to equation 2; (d) - radiated power fraction for stable plasmas.

Summary. The main profile diagnostics provide consistent parameters for the first W7-X campaign. Electron density profiles measured with Thomson scattering generally agree with the single channel interferometer, the difference is of about 10%. Electron temperatures measured with ECE, Thomson scattering and XICS are consistent within about 10% for discharges with low plasma pressure. For cases with higher plasma pressure a suitable mapping of ECE frequencies is under investigation. The kinetic energy, estimated from profile diagnostics, is about 25% higher than the diamagnetic energy, which is at least partially due to the unknown impurity content in the plasma.

The power balance is achieved within 10% of the heating power for heating powers less than about 1 MW and deteriorates up to 40% for 4 MW discharges. This can be caused by a toroidal asymmetry in the limiter heat fluxes. The radiated power fraction in stable plasma conditions for heating powers above 1 MW is about 30%, and is higher for lower powers.

The global energy confinement time τ_E for hydrogen discharges is at the level of the ISS04 scaling [11], which is about 150 ms. The confinement time shows a clear degradation with increasing radiated power fraction. It is to be noted, that the conditions in this campaign were not optimal: (i) limiters were located geometrically close to the core plasma and (ii) the magnetic configuration has an intrinsic $m/n = 6/5$ island chain and a further $5/4$ resonance in confinement region; (iii) also the full benefit of the optimisation of W7-X is predicted for higher densities. Therefore, a further improvement of the confinement time is expected for later campaigns.

Acknowledgment. This work has been carried out within the framework of the EUROfusion Consortium and has received funding from the Euratom research and training programme 2014-2018 under grant agreement No 633053. The views and opinions expressed herein do not necessarily reflect those of the European Commission.

[1] T. Sunn Pedersen et al. *Nuclear Fusion* **55** 126001
[2] S. Marsen et al. *this conference* **P4.002**
[3] T. Klinger et al. *this conference* **EV.001**
[4] D. Zhang et al. *this conference* **P4.015**
[5] E. Pasch et al. *this conference* **P4.016**
[6] M. Hirsch et al. *this conference* **P4.007**
[7] J. Knauer et al. *this conference* **P4.017**
[8] A. Langenberg et al. *this conference* **P4.014**
[9] K. Rahbarnia et al. *this conference* **P4.011**
[10] K. Niemann et al. *this conference* **P4.005**
[11] H. Yamada et al. *Nuclear Fusion* **45** 1684
[12] A. Hermann, *EPS* Vol. 25A, 2001
[13] G.A. Wurden et al. accepted to *RSI* 2016
[14] A. Dinklage et al. *this conference* **O2.107**